Transition Met Chem (2016) 41:435–445
DOI 10.1007/s11243-016-0039-2

Hydrolytic and redox transformations of chromium(III) bis-oxalato complexes with glutaminic acid and glutamine: a kinetic, UV–Vis and EPR, study

Emilia Kiersikowska[1] · Ewa Kita[1] · Przemysław Kita[1] · Grzegorz Wrzeszcz[1]

Received: 4 February 2016 / Accepted: 17 February 2016 / Published online: 1 March 2016

Abstract The title complexes have been synthesized, chromatographically isolated and characterized by their ligands to metal ratio determinations and spectroscopic analyses. The kinetics of the first aquation stage, i.e., the amino acid chelate ring opening via the Cr–N bond cleavage, has been studied spectrophotometrically in acidic and alkaline media. Hydrogen peroxide oxidizes the complexes in alkaline media to CrO_4^{2-} anion and a relatively stable Cr(V) complex. Consecutive biphasic kinetics through two first-order steps were observed for the base hydrolysis and the oxidation process, whereas the acid-catalyzed aquation obeys a simple first-order pattern. Based on the kinetic and spectroscopic data, mechanisms of the coordinated amino acid liberation and chromium(III) oxidation are discussed.

Introduction

For the last two decades, numerous dietary supplements for humans containing so-called biochromium have been offered. In fact, these pharmaceuticals contain only a few different chromium(III) complexes as active substances and all of them are recommended against obesity, arteriosclerosis and type II diabetes, e.g., [1–4]. Commercial success of the mentioned preparations seems to be independent of controversial discussion on the biological role of the chromium(III), e.g., [5–8]. On the other hand, there is no doubt that chromium species in higher oxidation states are toxic, carcinogenic and mutagenic. Particularly dangerous are chromium complexes at the intermediate oxidation states (IV) and (V). In the case of oxidative stress, Cr(III)-DNA adducts are oxidized to Cr(V) and CrO_4^{2-} anion. An overview of chromium redox transformations in biological systems is presented in [8]. In spite of this health risk, some recent reports point at possible application of selected chromium(III) complexes in medical therapy and diagnosis [9–12]. Very recent works on biological and medicinal aspects of chromium coordination chemistry include: (1) separation and speciation of chromium in chromium yeast [13], (2) syntheses, characteristics and biological activity of metforming drug for diabetes patients with chromium(III) [14] and (3) kinetic and mechanistic studies on Cr(V) → Cr(III) transformations [15–17]. As it was established, chromium(III) complexes being to the left of the "oxo wall", vide [18], can be involved not only in four-electron reduction of the oxygen, but also can act as selective catalysts in two-electron transformation of $O_2 \rightarrow H_2O_2$. In that case, chromium(V) can be the catalyst precursor. The latest findings [16] demonstrate the complexity of redox cycles of chromium in living organisms.

Very low bioavailability of commercial chromium(III) pharmaceuticals and their unknown mechanism in human administration still inspire chemists to look for new chromium(III) complexes and examine their chemical transformations. We studied chemical and biological activity of several chromium(III) complexes with amino acids, e.g., [19–21]. The present work deals with kinetics and mechanism of ligand substitution and redox transformations of chromium(III) bis-oxalato-glutaminic acid/glutamine complexes. While much work has been done on Cr(VI) → Cr(III) reduction, only a few articles have been published on mechanism of Cr(III) → Cr(VI) oxidation by

✉ Ewa Kita
ewakita@chem.umk.pl

[1] Nicolaus Copernicus University, Toruń, Poland

hydrogen peroxide. Glutamine (Gln), the ligand chosen in this work, is the most abundant free amino acid in the human body, 60 % of all free amino acids, and is involved in many metabolic processes. Production of Gln decreases with age, and external supplementation is recommended in such cases. It plays an anti-aging role, acts as a neurotransmitter, is used in medical treatments and also as a flavor enhancer (in the form of monosodium glutaminate, MSG), nutrient, plant growth preparation, etc. [22]. Speciation of the proteolytic forms of glutaminic acid and glutamine is shown in Scheme 1.

Two polynuclear chromium(III) complexes with glutaminic acid and glutamine or cysteine were isolated and physicochemically characterized before [23].

Experimental

Materials

Glutamine (Aldrich), glutaminic acid (Aldrich), $NaClO_4{\cdot}H_2O$ (Aldrich), 70 % $HClO_4$ (Aldrich) and other chemicals were used as supplied. Sephadex DEAE A-25 (ClO_4^-) and Sephadex C-25 (H^+) were used for chromatographic separations.

Preparation of $[Cr(ox)_2(Gln)]^{2-}$ and $[Cr(ox)_2(Glu)]^{2-}$ complexes

These complexes were prepared from trans-$K[Cr(ox)_2(H_2O)_2]{\cdot}3H_2O$ (2 mmol) and glutamine/glutaminic acid (3 mmol) according to the description given in [19]. The desired products were separated chromatographically using DEAE ion exchanger (ClO_4^-) with 0.2 M $NaClO_4$. The yield was ca. 40 %.

Spectroscopic characteristics of $[Cr(ox)_2(Gln)]^{2-}$ and $[Cr(ox)_2(Glu)]^{2-}$ complexes

Electronic Vis spectra of the complexes were recorded in aqueous solutions at pH 2. Values of molar absorption coefficients were calculated based on chromium concentration, which was determined spectrophotometrically as CrO_4^{2-} at 372 nm, after decomposition of the complexes (in $NaOH + H_2O_2$). Spectroscopic characteristics are given in Table 1.

Products of acid-catalyzed aquation

A solution of $[Cr(ox)_2(Gln)]^{2-}$ or $[Cr(ox)_2(Glu)]^{2-}$ (0.2 mmol) in 0.2 M $HClO_4$ (15 cm^3) was kept at 313 K for 30 min, i.e., time corresponding to 3 $t_{1/2}$, determined from the kinetic studies. Then, it was cooled, neutralized with cold 2.5 M KOH and kept in the refrigerator for 30 min. Next, the deposit of $KClO_4$ was filtered off, the solution was diluted to 100 cm^3 and introduced onto a column of anionic exchanger. Two species were eluted and identified as $[Cr(ox)_2(H_2O)_2]^-$ and $[Cr(ox)_2(Aa)]^{2-}$, respectively. Some chromium species were also found in the solution collected during sorption. As they did not exhibit affinity to the cationic exchanger, they were assumed to be $[Cr(ox)(Aa)(H_2O)_2]^0$. The composition of reaction mixtures obtained from acid-catalyzed aquation is given in Table 2.

Products of base hydrolysis

A solution of $[Cr(ox)_2(Gln)]^{2-}$ or $[Cr(ox)_2(Glu)]^{2-}$ (0.2 mmol) in 0.2 M KOH (15 cm^3) was kept at 303 K for 250 s. The reaction was quenched by addition of equimolar 2 M $HClO_4$ (using an ice bath), the precipitate was filtered

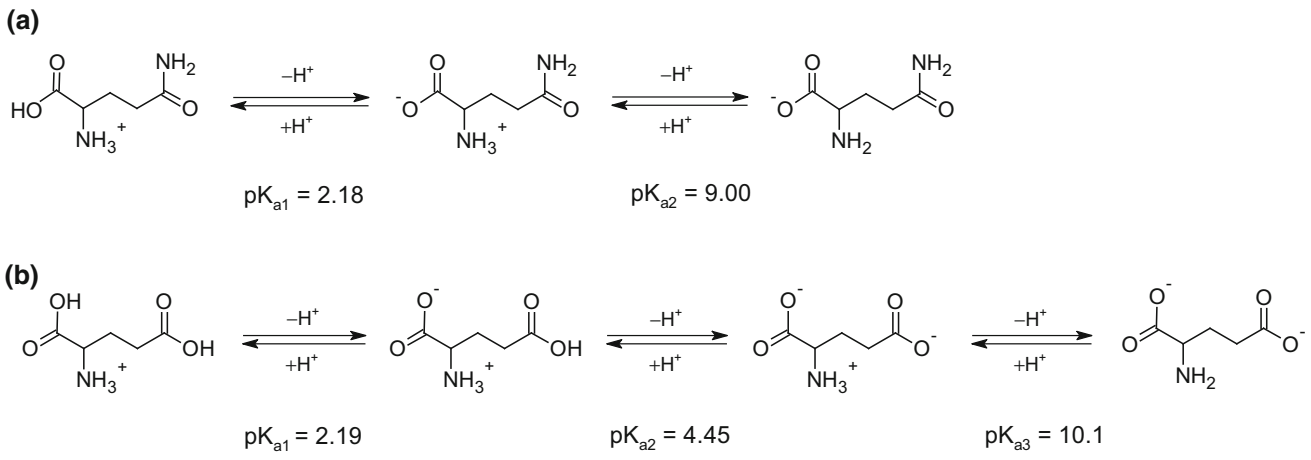

Scheme 1 Protolytic forms of glutamine (**a**) and glutaminic acid (**b**) in aqueous solution; the pK_a values at 298 K, $I = 0$ [8]

Table 1 Spectroscopic characteristics of $[Cr(ox)_2(Aa)]^{2-}$ in 0.01 $HClO_4$

Complex	λ_{max} (ε), nm ($M^{-1}cm^{-1}$)
$[Cr(ox)_2Gln]^{2-}$	406 (95) 549 (78)
$[Cr(ox)_2Glu]^{2-}$	406 (96) 549 (81)

Table 2 Composition of the reaction mixture obtained from acid-catalyzed aquation of $[Cr(ox)_2(Aa)]^{2-}$ at 313 K

Complex	*t* (min)	Composition of the reaction mixture (%)	
$[Cr(ox)_2Gln]^{2-}$	28	$[Cr(ox)_2Gln]^{2-}$	42
		$[Cr(ox)_2(H_2O)_2]^{-}$	39
		$[Cr(ox)(Gln)(H_2O)_2]^{0}$	9
$[Cr(ox)_2(Glu)]^{2-}$	28	$[Cr(ox)_2(Glu)]^{2-}$	45
		$[Cr(ox)_2(H_2O)_2]^{-}$	42
		$[Cr(ox)(Glu)(H_2O)_2]^{0}$	9

off, and the collected solution (diluted to 150 cm^3) was introduced onto a column of anionic exchanger. Only one colored complex (ca. 50 % of the total chromium content) eluted with 0.1 $HClO_4$ + 0.1 M $NaClO_4$ was obtained and identified as the substrate, $[Cr(ox)_2(Aa)]^{2-}$. The solution (practically colorless) collected during sorption (containing ca. 15 % of the total chromium content) was introduced onto the cationic exchanger, where only polynuclear μ-hydroxo-aquachromium(III) species were found. A quite large amount of chromium(III), ca. 40 % of the total chromium content, was found in the collected precipitate, which was analyzed spectrophotometrically as CrO_4^{2-}, after dissolution of chromium species present in the deposit in 0.4 M NaOH and oxidation by H_2O_2.

Spectroscopic evidence for formation of the metastable intermediate

Equal volumes (0.85 cm^3) of the complex solution and 0.4 M $HClO_4$ were placed in a tandem cell, respectively. The reaction was followed spectrophotometrically at 313 K for 3 $t_{1/2}$. In parallel, the same experiment was performed in a thermostated beaker and was quenched by the addition of an appropriate amount of 2.5 M KOH (pH 4–6). Positions of lower-energy *d–d* bands in the spectra of the mixtures at time 0 and 3 $t_{1/2}$ in acidic and neutralized reaction mixtures were compared (Table 3).

Kinetic measurements

Kinetics of the acid- and base-catalyzed aquation of the $[Cr(ox)_2(Gln)]^{2-}$ and $[Cr(ox)_2(Glu)]^{2-}$ complexes were studied spectrophotometrically (Spectrophotometer HP 8453 equipped with HP89090 Peltier temperature

Table 3 Position of lower-energy *d–d* transition band in the spectrum of reaction mixture of $[Cr(ox)_2(Aa)]^{2-}$ in 0.4 M $HClO_4$ and after pH increase

pH	$[Cr(ox)_2(Gln)]^{2-}$		$[Cr(ox)_2(Glu)]^{2-}$	
	t (min)	λ_{max} (nm)	*t* (min)	λ_{max} (nm)
1	0	549	0	549
1	14	566	15	564
7	14	556	15	554

controller) by monitoring the absorbance in the visible spectrum region, within the lower-energy *d–d* transition band. The concentration of $HClO_4$ and NaOH was varied between 0.2 and 1.0 M, and the ionic strength was 1.0 M ($NaClO_4$). Spectroscopic changes for $[Cr(ox)_2(Gln)]^{2-}$ are shown in Figs. 1 and 2 (spectroscopic changes for $[Cr(ox)_2(Glu)]^{2-}$ were practically the same).

The reaction was performed in 1-cm tandem cell, where equal volumes (0.85 cm^3) of the stock complex solution and the medium were mixed. Each kinetic run was performed for at least 3 $t_{1/2}$ of the substrate conversion and was repeated trice. Absorbance-time data obeyed a pseudo-first-order dependence for acid-catalyzed reactions. On the other hand, a consecutive reaction model, A → B → C, was applied for base hydrolysis. Values of pseudo-first-order rate constants, $k_{obs,H}$, were calculated from absorbance-time data collected at 550 nm using the Enzfitter program, and $k_{obs1,OH}$ and $k_{obs2,OH}$ were calculated by multifunctional analyses of scans recorded within 500–600 nm using SPECFIT software. The calculated k_{obs} were practically independent of the initial complex concentration.

Kinetics of oxidation of $[Cr(ox)_2(Gln)]^{2-}$ and $[Cr(ox)_2(Glu)]^{2-}$ were followed by the absorbance increase within the 350–400 nm spectral range (Fig. 3a). The concentration of oxidant, H_2O_2, was changed between 0.2 and

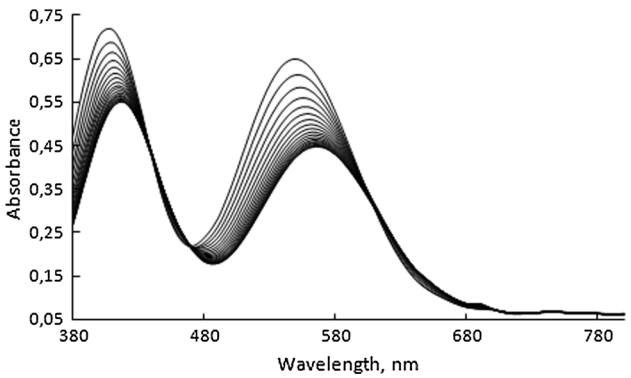

Fig. 1 Spectroscopic changes during aquation of $[Cr(ox)_2(Gln)]^{2-}$ in 0.6 M $HClO_4$; $[Cr(III)] = 8 \times 10^{-3}$ M, $I = 1$ M, $T = 303$ K, scans every 120 s

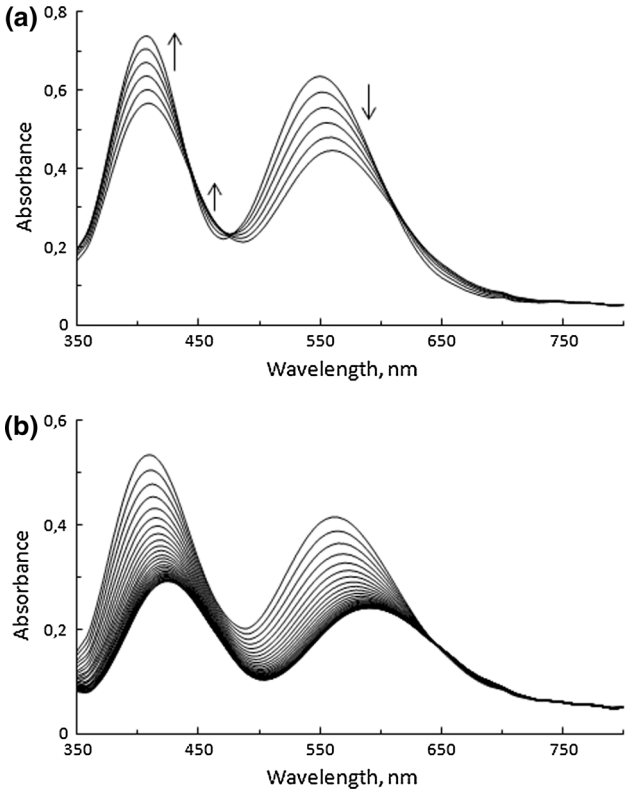

Fig. 2 Spectroscopic changes at the initial period (**a**) and after it (**b**) during base hydrolysis of $[Cr(ox)_2(Gln)]^{2-}$ in 0.6 M NaOH; [Cr(III)] = 8 × 10^{-3} M, I = 1 M, T = 303 K, scans every 40 s

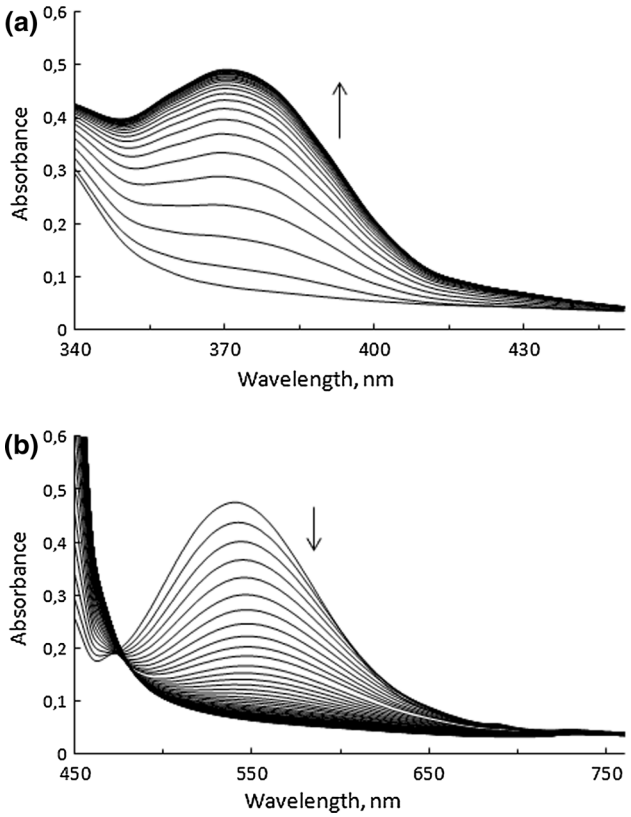

Fig. 3 Spectroscopic changes in the UV (**a**) and Vis (**b**) spectral range during oxidation of $[Cr(ox)_2(Gln)]^{2-}$ by H_2O_2 in 0.6 M NaOH; [Cr(III)] = 1.5 × 10^{-4} M (**a**) and 6.2 × 10^{-3} M (**b**), $[H_2O_2]$ = 0.2 M, T = 298 K, scans every 120 s (**a**) and 60 s (**b**)

1.0 M, the concentration of NaOH was kept constant at 0.6 M (taking into consideration neutralization of NaOH by H_2O_2), the concentration of chromium(III) was 1.5 × 10^{-4} M, and the ionic strength was 2.0 M ($NaClO_4$). The reaction was initiated by injection of 0.1 cm^3 of the complex solution into 1.9 cm^3 of the thermostated medium solution, prepared directly before the measurement from the appropriate amounts of NaOH and H_2O_2 stock solutions. Additionally some kinetic runs were performed in the Vis spectral range, using a 1-cm tandem cell (Fig. 3b).

Standard error of single pseudo-first-order rate constants, k_{obs}, was usually ca. 1 %, and that of the mean k_{obs} values was usually 1–2 %.

EPR measurements

EPR spectra of reaction mixtures, containing Aa-chromium(III) complexes and hydrogen peroxide in NaOH medium, were recorded with a Radiopan EPR SE/x2541 M spectrometer in X band (ca. 9.33 GHz) with 100-kHz modulation. The microwave frequency was monitored with an automatic NMR-type magnetometer. EPR spectra were recorded at room temperature, and the measurements were carried out from ca. 180 s after the initial mixing of reagents. A flat quartz cell was used. The solution concentrations were: [Cr(III)] = 1.5 × 10^{-4} M, $[H_2O_2]$ = 0.2 M, [NaOH] = 0.6 M. The initial intensity of EPR signal was relatively weak, but quickly increased during the reaction course, reaching a maximum within ca. 30 min (Fig. 4). At that point, the signal was stable for at least a few hours and

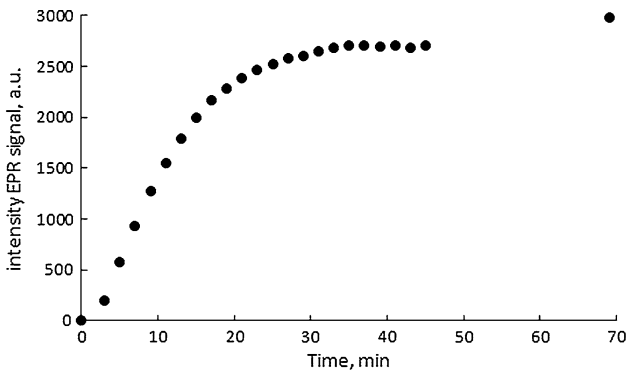

Fig. 4 Changes of intensity of EPR signal generated during oxidation of $[Cr(ox)_2(Gln)]^{2-}$ by 0.2 M H_2O_2 in 0.6 M NaOH at 298 K; [Cr(III)] = 1.5 × 10^{-4} M

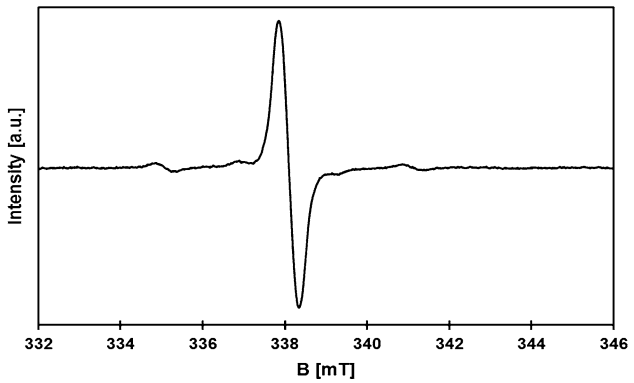

Fig. 5 EPR spectrum recorded for reaction mixture of 1.5×10^{-4} M $[Cr(ox)_2(Gln)]^{2-}$ and 0.2 M H_2O_2 in 0.6 M NaOH after 30 min from the initiation of the reaction; microwave frequency 9.33235 GHz, room temp

then slowly disappeared (within a few days or even weeks) due to decomposition of the hydrogen peroxide.

The chromium(V) EPR spectrum (Fig. 5) was identical with that recorded during oxidation of other chromium(III)-amino acid complexes by hydrogen peroxide [20, 21] and was assigned to $[Cr^{V}(O_2)_4]^{3-}$ species based on comparison of the obtained spectral parameters with the literature data [24, 25]: a strong isotropic signal due to chromium isotopes with $I = 0$ (90.5 %) at $g_{iso} = 1.9722 \pm 0.0003$ and peak-to-peak width, DBpp $\times$ 0.2 mT. A small isotropic satellite signal, split into a quartet due to hyperfine coupling by the less abundant (9.5 %) ^{53}Cr isotope ($I = 3.2$), is also observed with a $(^{53}Cr) = 18.59 \times 10^{-4}$ cm^{-1} [24, 25].

Results and discussion

Two new complexes, $[Cr(ox)_2(Gln)]^{2-}$ and $[Cr(ox)_2(Glu)]^{2-}$, were obtained via anation of *cis*-$[Cr(ox)_2(H_2O)_2]^{-}$ by glutamine and glutaminic acid followed by chromatographic separation. Electronic spectra of the complexes within *d–d* transition range (Table 1) are practically the same as those for analogous complexes with other amino acids [19–21] and are consistent with bidentate N,O-coordination of the amino acid. Substitution of H_2O ligands by Gln/Glu in the starting complex results in ca. 10-nm blueshift of the lower-energy *d–d* band and an intensity increase. The absence of H_2O ligands in the coordination sphere of the anation products was confirmed by independence of their spectra of pH within the 1–13 range, recorded immediately after preparation of the complexes solution.

Aquation of the complexes is conveniently monitored by spectral changes in strongly acidic (Fig. 1) or strongly alkaline media (Fig. 2). In neutral solutions, both the complexes are very inert.

Acid-catalyzed aquation of $[Cr(ox)_2(Glu)]^{2-}$ and $[Cr(ox)_2(Gln)]^{2-}$

The rate of aquation in acidic media increases with the concentration increase of H^{+}_{aq} and leads to liberation of the amino acid. The parallel process, dissociation of oxalate, takes place in much smaller extent; the molar ratio of the bis-oxalato to mono-oxalato products is ca. 10 (Table 2). Moreover, spectral changes accompanying oxalato ligand dissociation are much smaller than those accompanying the amino acid liberation, and for this reason absorbance-time data can be attributed only to reaction (1):

$$[Cr(ox)_2(Gln)]^{2-} + 2H_2O + H^{+} \rightarrow \left[Cr(ox)_2(H_2O)_2\right]^{-} + GlnH \quad (1)$$

Formation of the diaqua product (Eq. 1) results in absorbance decrease in the whole visible region and a redshift of the $^4A_{2g} \rightarrow {}^4T_{2g}$ transition (pseudo-O_h symmetry approximation) (Fig. 1). The presence of isosbestic points at 439, 467 and 610 nm (for both the Gln/Glu-complexes) during the reaction course (up to 0.9 of the conversion degree) indicates that only one step from the two steps of amino acid dissociation is observed spectrophotometrically. Additionally performed experiments (vide Experimental) revealed cumulation of the intermediate complex, $[Cr(ox)_2(AaH)(H_2O)]^{-}$ (where AaH is coordinated through the carboxylate oxygen atom), in the reaction mixture (Table 2). This intermediate is metastable in acidic media, but undergoes fast conversion into the substrate upon neutralization, manifested by a blueshift of the lower-energy *d–d* transition band in the spectrum of the reaction mixture after 3 $t_{1/2}$ if pH increases from 1 to 7. Thus, the first step of the amino acid dissociation, the chelate ring opening at the Cr–N bond, is faster than liberation of the one-end bonded amino acid.

Absorbance-time data obey a first-order kinetics at constant $[H^{+}]$. Values of the pseudo-first-order rate constants are shown in Table 4, and their acid dependence is presented in Fig. 6.

The chelate ring-opening process is catalyzed by H^{+}, and the k_{obs} increases linearly with $[H^{+}]$ increase (Eq. 2):

$$k_{obs} = a + b[H^{+}] \quad (2)$$

Values of the *a* and *b* parameters and the activation parameters, calculated from the *b* parameter, are given in Table 5.

Based on the obtained results (identified reaction intermediates and products, spectroscopic and kinetic data), the following reaction mechanism can be proposed (Scheme 2).

Table 4 Dependence of k_{obs} on $[H^+]$ for acid-catalyzed aquation of $[Cr(ox)_2(Gln)]^{2-}$ (A) and $[Cr(ox)_2(Glu)]^{2-}$ (B)

$[H^+]$, M	$10^3 k_{obs}$ (s^{-1}) 303 K	$10^3 k_{obs}$ (s^{-1}) 313 K	$10^3 k_{obs}$ (s^{-1}) 323 K
(A)			
0.2	–	1.35 ± 0.04	3.64 ± 0.17
0.4	0.852 ± 0.037	2.34 ± 0.07	6.12 ± 0.19
0.6	1.35 ± 0.09	3.52 ± 0.05	9.18 ± 0.30
0.8	1.86 ± 0.19	4.72 ± 0.13	12.5 ± 0.32
1.0	2.24 ± 0.15	5.25 ± 0.19	–
(B)			
0.1	–	–	1.80 ± 0.05
0.2	0.472 ± 0.038	1.28 ± 0.18	3.29 ± 0.12
0.4	0.803 ± 0.003	2.25 ± 0.05	5.68 ± 0.16
0.6	1.19 ± 0.06	3.29 ± 0.05	8.26 ± 0.12
0.8	1.61 ± 0.01	4.34 ± 0.05	11.2 ± 0.3
1.0	2.04 ± 0.13	5.49 ± 0.23	–

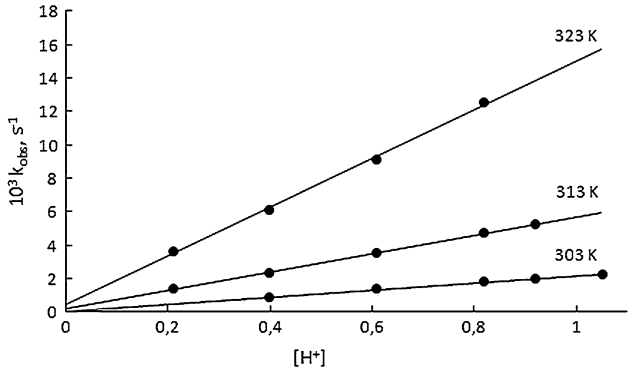

Fig. 6 Dependence of k_{obs} on $[H^+]$ for acid-catalyzed aquation of $[Cr(ox)_2(Gln)]^{2-}$

The acid-catalyzed reaction path predominates in strongly acidic media. This process is initiated by protonation of the coordinated carboxylic group (SH) leading to destabilization of the chelate ring, which results in the Cr–N bond cleavage and formation of the monoaqua intermediate, $P_{1,Aa}$. The rate law derived from the presented reaction model is of the form:

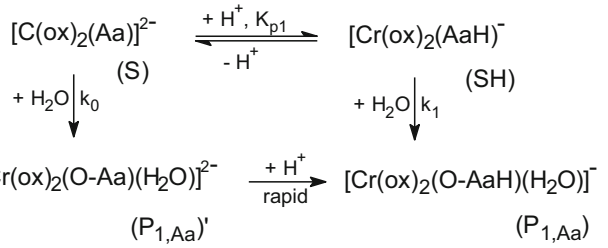

Scheme 2 Mechanism for the first stage of amino acid dissociation from $[Cr(ox)_2(Aa)]^{2-}$

$$k_{obs1} = (k_0 + k_1 K_{p1}[H^+])/(1 + K_{p1}[H^+]) \quad (3)$$

If the protolytic equilibrium is shifted left, i.e., $K_{p1}[H^+] \ll 1$, Eq. 3 simplifies to the observed linear dependence k_{obs1} on $[H^+]$:

$$k_{obs1} = k_0 + k_H[H^+] \quad (4)$$

where $k_H = k_1 K_{p1}$.

Thus, comparison of Eq. 2 with Eq. 4 gives mechanistic interpretation of the experimental parameters a and b:

$$a = k_0 \text{ and } b = k_H = k_1 K_{p1}. \quad (5)$$

The apparent activation parameters, shown in Table 5, are the sums of activation enthalpy (entropy) of the chelate ring-opening process and enthalpy (entropy) of the chelate ring protonation. An analogous mechanism operates for H^+-catalyzed aquation of other chromium(III) bis-oxalato complexes with amino acids [19]. Comparison of the rate data (the pseudo-second-order rate constants, b parameter) leads to the conclusion that the side chain of α-amino acids plays a minor role in determination of the complex reactivity. Values of the $10^3 b$ $[M^{-1}s^{-1}]$ at 298 K, $I = 1.0$ M are as follows: 0.84 (Val), 0.96 (Asp), 0.99 (Cys), 1.08 (Glu), 1.20 (Gln), 1.21 (Ala), 1.58 (His), 1.64 (Ser) [19]. Values of the apparent activation parameters for these complexes are quite similar; $\Delta H^{\neq}$ is usually 74–80 kJ mol^{-1} and $\Delta S^{\neq}$ is near −50 eu, which clearly indicates an analogous mechanism for all $[Cr(ox)_2(Aa)]^{2-}$ complexes.

Hydrolytic Cr–N bond cleavage in H^+-catalyzed reaction paths for $[Cr(Gly)_3]^0$ and $[Cr(Asp)_2]^-$ complexes is

Table 5 Values of the a and b parameters (Eq. 2) determined for the acid-catalyzed aquation of $[Cr(ox)_2(Aa)]^{2-}$ and activation parameters at 298 K for the Cr–Aa ring opening calculated from the b parameters

	$[Cr(ox)_2(Gln)]^{2-}$		$[Cr(ox)_2(Glu)]^{2-}$	
	10^3 a (s^{-1})	10^3 b (s^{-1} M^{-1})	10^3 a (s^{-1})	10^3 b (s^{-1} M^{-1})
303 K	0.036 ± 0.089	2.13 ± 0.11	0.063 ± 0.016	1.88 ± 0.02
313 K	0.160 ± 0.031	5.54 ± 0.05	0.241 ± 0.011	5.00 ± 0.02
323 K	0.427 ± 0.273	14.6 ± 0.49	0.476 ± 0.089	13.0 ± 0.2
298 K	0.028	1.20	0.059	1.08
$\Delta H^{\neq}$ (kJ/mol)	85 ± 8	78 ± 1	65 ± 12	77.1 ± 0.6
$\Delta S^{\neq}$ (J/mol K)	−47 ± 25	−41 ± 4	−11 ± 38	−43 ± 2

faster than that for the bis-oxalato complexes; values of the 10^3 b [$M^{-1}s^{-1}$] at 298 K are 4.5 and 8.4, respectively [26, 27]. Thus, oxalato ligands slightly retard the amino acid chelate ring-opening process.

Base hydrolysis of $[Cr(ox)_2(Glu)]^{2-}$ and $[Cr(ox)_2(Gln)]^{2-}$

In strongly alkaline media (pH > 13), both the complexes undergo relatively slow ligand dissociation to give chromates(III). Chromatographic separations of the neutralized reaction mixture obtained after $t_{1/2}$ of the substrate conversion revealed the starting complex and greenish polynuclear μ-hydroxo-aquachromium(III). Spectroscopic changes during the reaction course (Fig. 2) are characteristic for a two-step process. At the first step (Fig. 2a), ca. 50 % of absorbance decrease, sharp isosbestic points (at 440, 478 and 607 nm for the Gln/Glu-complex) are held very well, then (Fig. 2b) they disappear, and further absorbance decrease and a redshift are observed. In spite of substantial spectroscopic changes during the first reaction step (λ_{max} 550 → 557 nm, A_{max} 0.6 → 0.4), neutralization of the reaction mixture causes practically complete reverse of the spectrum to that at $t = 0$ s. These results are consistent with parallel chelate rings opening via the Cr–N and Cr–ox bond cleavage and formation of the $[Cr(ox)_2(Gln')(OH)]^{3-}$ and $[Cr(ox)(ox')(Gln)(OH)]^{3-}$ or $[Cr(ox)_2(Glu')(OH)]^{4-}$ and $[Cr(ox)(ox')(Glu)(OH)]^{4-}$ (Glu is dianionic because of its two carboxylate groups) intermediates. Then ligands substitution takes place. The back reaction is insignificant at pH > 13, because the monoaqua intermediate is deprotonated and the hydroxido ligand blocks the chelate ring closure. Lack of $[Cr(ox)_2(H_2O)_2]^-$ and Gln/Glu-tetraaquachromium(III) complex in the acidified reaction mixture indicates that both ligands, oxalato and Aa, are liberated with similar rates.

Kinetics of the base hydrolysis were examined using SPECFIT software for scans registered within the 500–600 nm region for the consecutive first-order A → B → C reaction model. The calculated values of the k_{obs1} and k_{obs2} are collected in Table 6.

As it is seen, values of the first-order rate constants for both the stages are only slightly dependent on [OH^-] and therefore we calculated only one average value for k_{obs1} and k_{obs2} at each temperature studied (Table 7). It is also seen that the k_{obs1} values are ca. twice higher than those for k_{obs2}. The presented data are consistent with the reaction mechanism shown in Scheme 3.

In the stage I, two parallel reactions—the chelate ring opening at Cr–ox and Cr–Aa—take place and monohydroxido intermediates, $[Cr(ox)_2(Aa')(OH)]^{3-}$ ($P_{1,OH}$) and $[Cr(ox)(ox')(Aa)(OH)]^{3-}$ ($P_{2,OH}$)', are formed. The presence of these two intermediates is consistent with a relatively small redshift (ca. 10 nm) of the lower-energy d–d band which is much smaller than that expected for substitution of only the N-donor atom by the OH^- ligand. These intermediates are assumed to be in comparable amounts. Thus, the determined k_{obs1} rate constants are sums of the rate constants:

$$k_{obs1} = k_1' + k_1'' \quad (6)$$

As it was mentioned, neutralization of the reaction mixture at the first reaction stage reverses the hydrolysis and the initial complex is restored. In the second stage, monodentate bonded ligands (Aa' and ox') are liberated and then decomposition of the complexes leading to chromates(III) takes place. Thus, the k_{obs2} values are also sums of the rate constants for spontaneous one-end bonded ligand (Aa' and ox') liberation.

$$k_{obs2} = k_2' + k_2'' \quad (7)$$

Values of apparent activation parameters are given in Table 7.

Comparison of the $k_{obs1,H}$ in 1 M $HClO_4$ (ca. 2×10^{-3} s^{-1}) and $k_{obs1,OH}$ (ca. 8×10^{-3} s^{-1}) determined at 303 K shows that the rates of the first reaction stage markedly depend on medium; in acidic solution, the process is slower than in alkaline medium. Rationalization of this kinetic effect can be based on hindrance of the reverse process, i.e., the chelate ring closure by hydroxido ligand in monohydroxido intermediates.

It seems to be remarkable that the $k_{obs1,OH}$ values are higher than those of the $k_{obs2,OH}$ in spite of the presence of OH^- ligand in the coordination sphere which labilizes the complex. Determined values of $(\Delta S^{\neq})_1$ and $(\Delta S^{\neq})_2$ are apparent activation parameters because they are the sums of activation entropies for two parallel processes. High negative values of the activation entropies for both the reaction stages suggest an associative mode of the transition state formation classified as I_A-type mechanism. For dissociative mode of activation, expected increase of hydration leading to the entropy decrease would be counterbalanced by entropy increase caused by Cr–L bond breaking, resulting in close to zero entropy value.

Oxidation of $[Cr(ox)_2(Aa)]^{2-}$ by H_2O_2

Oxidation of the bis-oxalato complexes with Gln and Glu, and additionally also $[Cr(ox)_2(H_2O)_2]^-$ and $[Cr(ox)(H_2O)_4]^+$, carried out under a large excess of H_2O_2 and OH^- was monitored spectrophotometrically within the UV–Vis range and additionally using EPR technique. This process is quite slow with the exception of $[Cr(ox)(H_2O)_4]^+$ oxidation; spectroscopic changes take place for ca. 30 min at 298 K. Two chromium species at higher oxidation states, i.e., CrO_4^{2-} anion and Cr(V) identified as $[Cr(O_2)_4]^{3-}$, are

Table 6 Dependence of k_{obs1} and k_{obs2} on [OH^-] for base hydrolysis of $[Cr(ox)_2(Gln)]^{2-}$ (A) and $[Cr(ox)_2(Glu)]^{2-}$ (B)

[OH^-] M	$10^3 k_{obs1}$ (s^{-1})			$10^3 k_{obs2}$ (s^{-1})		
	293 K	303 K	313 K	293 K	303 K	313 K
A						
0.2	2.76 ± 0.15	7.91 ± 0.14	18.2 ± 1.3	1.45 ± 0.004	3.94 ± 0.08	9.75 ± 0.15
0.4	2.80 ± 0.07	8.16 ± 0.70	18.8 ± 1.2	1.56 ± 0.06	3.93 ± 0.28	10.4 ± 0.44
0.6	3.02 ± 0.11	8.08 ± 0.30	19.6 ± 1.3	1.58 ± 0.06	4.21 ± 0.07	10.5 ± 0.4
0.8	2.92 ± 0.19	8.10 ± 0.10	19.5 ± 0.4	1.64 ± 0.44	4.46 ± 0.11	11.0 ± 0.4
0.9	2.97 ± 0.25	8.19 ± 0.33	20.8 ± 0.9	1.67 ± 0.25	4.56 ± 0.07	10.9 ± 0.1
B						
0.2	–	6.88 ± 0.38	17.2 ± 1.2	–	3.76 ± 0.04	9.38 ± 0.13
0.4	2.60 ± 0.13	7.33 ± 0.60	18.4 ± 0.3	1.48 ± 0.03	3.97 ± 0.12	10.0 ± 0.2
0.6	2.98 ± 0.12	7.81 ± 0.55	19.5 ± 1.4	1.48 ± 0.01	4.06 ± 0.03	10.3 ± 0.4
0.8	2.71 ± 0.47	8.70 ± 0.64	18.2 ± 0.5	1.62 ± 0.13	4.14 ± 0.08	10.5 ± 0.4
0.9	2.88 ± 0.25	8.10 ± 0.72	17.8 ± 1.0	1.59 ± 0.01	4.29 ± 0.02	11.2 ± 0.3

Table 7 Values of the k_{obs1} and k_{obs2} and activation parameters at 298 K determined for base hydrolysis of $[Cr(ox)_2(Aa)]^{2-}$

	$[Cr(ox)_2(Gln)]^{2-}$		$[Cr(ox)_2(Glu)]^{2-}$	
	10^3 k_{obs1} (s^{-1})	10^3 k_{obs2} (s^{-1})	10^3 k_{obs1} (s^{-1})	10^3 k_{obs2} (s^{-1})
293 K	2.89 ± 0.13	1.58 ± 0.11	2.79 ± 0.27	1.54 ± 0.10
303 K	8.08 ± 0.14	4.22 ± 0.32	7.76 ± 0.87	4.04 ± 0.27
313 K	19.4 ± 1.32	10.5 ± 0.63	18.2 ± 1.6	0.3 ± 0.92
298 K	4.98	2.61	4.81	2.50
$\Delta H^{\neq}$ (kJ/mol)	68.1 ± 1.9	69.6 ± 0.2	66.6 ± 2.2	70.9 ± 0.7
$\Delta S^{\neq}$ (J/mol K)	−61.1 ± 6.1	−60.7 ± 0.6	−65.7 ± 7.2	−56.9 ± 2.1

Scheme 3 Mechanism of base hydrolysis of $[Cr(ox)_2(Aa)(H_2O)_2]^{2-}$; Aa′ and ox′ denote one-end bonded ligand through oxygen atom

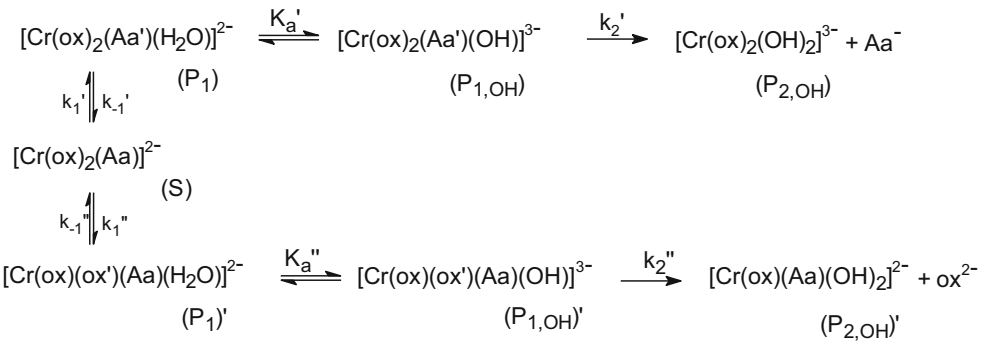

observed practically from beginning of the reaction (Figs. 3, 4). Distribution of Cr(VI) and Cr(V) species can be evaluated from the spectra shown in Fig. 3. As it is seen, at the "end" of the reaction ca. 35 % of chromium is in the form of the metastable chromium(V), which practically does not absorb within the monitored spectral range at 10^{-4} M total concentration of chromium.

The rate parameters can be determined from the absorbance increase at 372 nm (the λ_{max} for CrO_4^{2-}), from EPR signal intensity increase (formation of Cr^V) or from absorbance decrease within the *d–d* transition region (Cr^{III} disappearance). The later method is less convenient because it requires two orders of magnitude higher substrate concentration, causing additional complication due to oligomerization of Cr(III) species [28]. For this reason, kinetic measurements were done at low Cr(III) concentration, in the UV region, and only in a few cases, the obtained results were compared with those obtained from visible spectra and from EPR data. Multiwavelength analysis of the absorbance-time data shows that reaction is biphasic and proceeds through two consecutive first-order steps. Similar results including values of the rate constants were obtained from visible range data and EPR signal intensity changes with time. Thus, the rates of CrO_4^{2-} and

Cr(V) formation and the rate of Cr(III) disappearance are practically equal. The data were processed using a consecutive first-order A → B → C reaction pattern with the help of SPECFIT software. Additionally, absorbance-time data collected after 300 s for oxidation of the Gln- and Glu-complexes and after 100 s for $[Cr(ox)_2(H_2O)_2]^-$ were fitted to a simple first-order A → B reaction model. Calculated values of the pseudo-first-order rate constants are shown in Table 8.

Analogous consecutive biphasic kinetics for base hydrolysis and the oxidation process and very close values of the rate constants for two stages (especially those for the second one) for both the reactions (Tables 7, 8) firmly confirm the importance of ligand substitution during oxidation. Electron transfer from Cr(III) leading to Cr(V) and CrO_4^{2-} is preceded by chelate ring opening and then one-end bonded ligand liberation. The above-mentioned arguments and determined equal rates of Cr(III) disappearance and formation of $[Cr^V(O_2)_4]^{3-}$ and CrO_4^{2-} can be rationalized assuming the following simplified reaction scheme for $[Cr(ox)_2(Aa)]^{2-}$ oxidation (Scheme 4).

The rate controlling steps of the overall redox process are substitution reactions, i.e., formation of the monohydroxido and dihydroxido derivatives: $(P_{1,OH})$ $(P_{2,OH})$ $(P_{1,OH})'$ and $(P_{2,OH})'$, expressed by the rate constants $k_1' + k_1''$ for the first oxidation stage and by the sum $k_2' + k_2''$ for the second stage. In the subsequent faster steps, hydrogen peroxide is coordinated to the Cr(III) center as hydroperoxido anion forming two types of redox active intermediates, $I_{1,OOH}$ and $I_{2,OH,OOH}$ which generate Cr^VO via the inner-sphere two-electron transfer from the HOMO π* Cr(III) d orbital into the LUMO σ* hydroperoxido orbital. All individual rate constants for electron transfer are approximated by a common k_{et} rate constant (Scheme 4). The formed Cr^VO is further transformed in two fast parallel reaction paths: (1) It decays by disproportionation, and (2) its coordination sphere is rearranged by ligands exchange giving long-lived $[Cr^V(O_2)_4]^{3-}$. The ratio of rate constants for these two fast reaction paths determines the relative content of CrO_4^{2-} and $[Cr^V(O_2)_4]^{3-}$ in the reaction mixture. EPR measurements at low hydrogen peroxide concentration revealed that chromium(V) not stabilized by a large excess of $[H_2O_2]$ decays fast, forming finally CrO_4^{2-} anion.

Some other data presented in Table 8 can be considered as helpful in elucidation of the oxidation mechanism. A small but systematic increase of the k_{obs1} value with the $[H_2O_2]$ increase suggests that the equilibrium leading to an $I_{1,OOH}$-type an intermediate is not completely shifted to the right and moreover, the value of the rate for the intramolecular electron transfer (k_{et}) is comparable with $k_1' + k_1''$. However, the predominant reaction path is that through $I_{2,OH,OOH}$-type intermediate and for that reason kinetics of the overall oxidation process can be satisfactorily described by a simple A → B model, if the initial part of the reaction is omitted. This conclusion is supported by the very close values of k_{obs2} and k_{obs} (Table 8). Practically equal values of the rate constants for the second step of the base hydrolysis (Table 7) and the oxidation (Table 8) support the assumption that ligand liberation is the rate-limiting step for the second oxidation stage and thus $k_2' + k_2'' \ll k_{et}$. Interestingly, the value of k_{obs} for

Table 8 Dependence of k_{obs} on $[H_2O_2]$ during oxidation of $[Cr(ox)_2(Gln)]^{2-}$ (A) and $[Cr(ox)_2(Glu)]^{2-}$ (B), $[Cr(ox)_2(H_2O)_2]^-$ (C) and $[Cr(ox)(H_2O)_4]^+$ (D) in 0.6 M NaOH at 298 K

Complex	$[H_2O_2]$, M	10^3 k_{obs} (s^{-1})[a]	10^3 k_{obs1} (s^{-1})[b]	10^3 k_{obs2} (s^{-1})[b]
A	0.2	2.04 ± 0.04	6.28 ± 0.06	2.36 ± 0.01
	0.4	2.20 ± 0.05	6.52 ± 0.12	2.56 ± 0.01
	0.6	2.40 ± 0.08	7.34 ± 0.16	2.60 ± 0.01
	0.8	2.54 ± 0.06	8.22 ± 0.17	2.70 ± 0.01
	1.0	2.70 ± 0.06	9.93 ± 0.31	2.69 ± 0.01
B	0.2	1.94 ± 0.05	7.24 ± 0.22	2.20 ± 0.01
	0.4	2.01 ± 0.12	9.07 ± 0.37	2.14 ± 0.01
	0.6	2.08 ± 0.06	8.45 ± 0.41	2.28 ± 0.01
	0.8	2.20 ± 0.05	7.41 ± 0.22	2.50 ± 0.02
	1.0	2.36 ± 0.09	9.02 ± 0.26	2.50 ± 0.01
C	0.2	0.873 ± 0.014		
	0.8	0.894 ± 0.012		
	1.0	0.918 ± 0.022		
D	0.2	51 ± 4		

[a] Data calculated for A → B model from spectra recorded at 300–1500 s for A and B and at 100–2500 s for C

[b] Data calculated for A → B → C model from spectra recorded at 60–2000 s for A and B

Scheme 4 Mechanism of oxidation of $[Cr(ox)_2(Aa)]^{2-}$ by H_2O_2 in NaOH medium

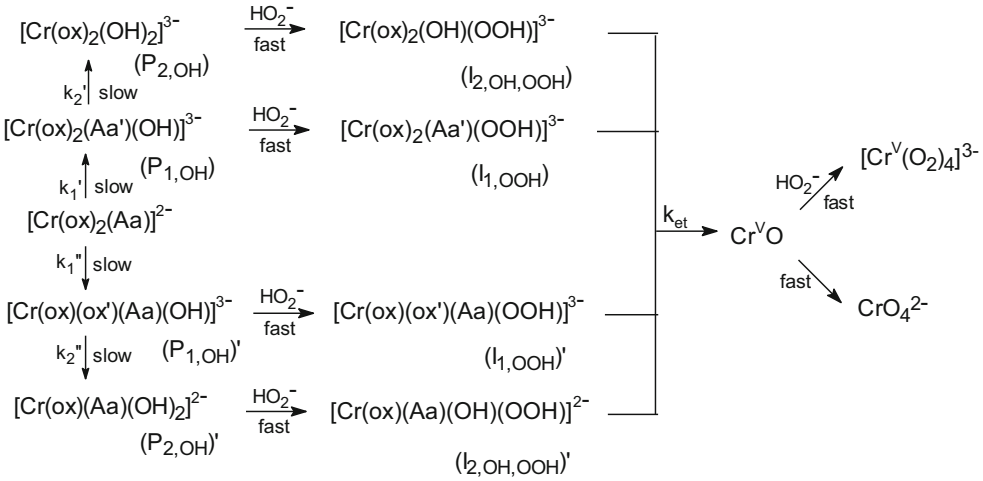

$[Cr(ox)_2(H_2O)_2]^-$ is twice lower than that for $[Cr(ox)_2(Aa)]^{2-}$ (Table 8) though in this case chromium(III)-oxalato ring opening and then the ligand liberation is not a necessary prerequisite for formation of the redox active intermediates of the Cr(III)–OOH type. In this case, the rate constant, k_{et}, controls the rate of the overall oxidation process.

Very close values of the analogous k_{obs} for $[Cr(ox)_2(Aa)]^{2-}$ studied and lower k_{obs} values for $[Cr(ox)_2(H_2O)_2]^-$ imply that the presence of an amino acid in the inner coordination sphere accelerates the electron transfer. The much higher rate constant for oxidation of $[Cr(ox)(H_2O)_4]^+$ (Table 8) comparable to that for chromates(III) [29] demonstrates redox lability of chromium complexes with four or more unblocked coordination sites.

Conclusions

The first aquation stage of $[Cr(ox)_2(Gln)]^{2-}$ and $[Cr(ox)_2(Glu)]^{2-}$ complexes in acidic and alkaline media proceeds through parallel reaction paths, namely the Cr–O bond cleavage in the Cr(III)-oxalato chelate ring and the Cr–N bond fission in the Cr(III)–Gln/Glu chelate rings. In acidic media, this reaction stage is $[H^+]$ catalyzed and proceeds mainly through the Cr–N bond cleavage, whereas at pH > 13 it is practically $[OH^-]$ independent and the rates of both the chelate rings opening are similar. The chelate ring opening in complexes without an aqua-ligand in the inner coordination sphere is *conditio sine qua non* for Cr(III) oxidation by hydrogen peroxide. However, the oxidation rate is also controlled by intramolecular electron transfer within the Cr(III)–OOH- and Cr(III)(OH)–OOH-type intermediates. Their reactivities are quite similar, whereas those for complexes with a larger number of hydroxido ligands are much higher. Thus, chromium(III) complexes with four unblocked coordination sites are oxidized rapidly by hydrogen peroxide in alkaline media.

References

1. Anderson RA (1998) J Am Coll Nutr 17:548
2. Slesinski RS, Clarke JJ, San RHC, Gudi R (2005) Mutation Res 585:86
3. Nielsen FH (2007) Summary: the clinical and nutritional importance of chromium—still debated after 50 years of research. In: Vincent JB (ed) The nutritional biochemistry of chromium(III). Elsevier, Amsterdam, pp 265–276
4. Levina A, Lay PA (2005) Coord Chem Rev 249:281
5. Gabriel C, Raptopoulou CP, Terzis A, Tangoulis V, Mateescu C, Salifolou A (2007) Inorg Chem 46:2998
6. Vincent JB (2010) Dalton Trans 39:3787
7. Alessio E (20111) Bioinorganic medicinal chemistry. Willey-VH, Vienheim, pp 343–365
8. Sharma VK (2013) Oxidation of amino acids, peptides, and proteins. Willey, New Jersey, pp 279–302
9. Wang ZQ, Cefalu WT (2010) Cur Diabetes Rep 10:145
10. Cefalu WT et al (2010) Metab, Clin Exp 59:755
11. Kelly JN et al (2010) Dalton Trans 39:3990
12. Wheller JF et al (2010) Inorg Chem 49:839
13. Guo X, Liu W, Bai X, He X, Zhang B (2014) World J Microbiol Biotechnol 30:3245
14. Adam AMA, Sharshar T, Mohamed MA, Ibrahim OB, Refat MS (2015) Spectrochim Acta Part A Mol Biomol Spectrosc 149:323
15. Cho J et al (2014) Inorg Chem 53:645
16. Abu-Omar MM et al (2014) Inorg Chem 53:7780
17. Kotani H et al (2015) Chem Sci 6:945
18. Winkler JR, Gray HB (2011) Struct Bond (Berlin, Ger) 142:17
19. Kita E et al (2012) Transition Met Chem 37:337

20. Kita E et al (2013) Transition Met Chem 38:603
21. Kita E et al (2014) Transition Met Chem 39:361
22. http://www.amino-acids/glutamineandglutaminicacid
23. Cieślak-Golonka et al (2002) Transition Met Chem 27:473
24. Dalal NS, Millar JM, Jagadeesh MS, Seehra MS (1981) J Chem Phys 74:1969
25. Zhang L, Lay PA (1998) Inorg Chem 37:1729
26. Kita E et al (2011) Transition Met Chem 35:44
27. Kita E et al (2014) Transition Met Chem 39:63
28. Torapava N, Radkevich A, Davytov O, Titov A, Pearsson I (2009) Inorg Chem 48:10383
29. Impert O, Katafias A, Kita P, Woroniecka M (2008) Polish J Chem 82:1121